Comparison of Model Reference Control Schemes for Motor Speed Control Under Variable Load Torque

Jessica VILLALOBOS[1]*, Fernando MARTELL[1], Irma Y. SANCHEZ[2]

[1] Centro de Investigaciones en Optica, 607 Prol. Constitucion, Aguascalientes, 20200, Mexico
jessicavillalobos@cio.mx (**Corresponding author*), fmartell@cio.mx

[2] Ingenieria Mecatronica S.A. de C.V., 204 Cordoba, Aguascalientes, 20235, Mexico
isanchez@ingmt.com

Abstract: Accurate motion control is required in mechatronic and robotic systems and is particularly important when the inverse kinematic control of robotic manipulators is done by controlling each joint independently; for this reason, it is necessary to find methods to optimize the position control strategies used in robotics, which can be achieved by focusing on controlling the speed of actuators. Controlled DC motors should be tested under extreme conditions for such applications. Performance indices pertaining to actuator wear-out and control accuracy are used for the evaluation. This study proposes a speed control strategy for a direct current motor that uses a model reference control (MRC) scheme and combines it with an internal model control (IMC) based proportional-integral (PI) controller. Three different controllers are used in the MRC to compare the performance of the proposed strategy with an IMC-based PID (Proportional Integral Derivative) controller in numerical simulations. For the experimental tests, particular tuning parameters are presented for the PID to control a DC motor when only a first-order model is identified. The proposed MRC-IMC scheme imposes a first-order response to the actuator while compensating for disturbances caused by load torque variations. Simulation and experimental results validate a better performance of the proposed control strategy.

Keywords: Independent joint control, Internal model principle, Model reference control, DC motor speed control.

1. Introduction

Optimizing speed and position control schemes is important because motion control of mechatronic technologies used in manufacturing systems affects product quality. There are several investigations on motion control of actuators (Dermitas, 2011; Ren et al., 2022), some of which use model-based controllers (MBCs) (Arenas-Rosales, Martell-Chávez & Sánchez-Chávez, 2022; Najafi & Spencer Jr., 2019). Additional control strategies are implemented to handle modeling uncertainties (Yao, Jiao & Ma, 2014) and obtain better trajectory tracking performance (Zhen et al., 2022).

The direct synthesis (Kumar, Singla & Chopra, 2015) and lambda tuning (Normey-Rico & Camacho, 2007) methods are well-known tuning techniques; however, the IMC, which is an MBC, can also be used to tune proportional-integral-derivative (PID) controllers (Rivera, Morari & Skogestad, 1986) and has inspired other rules (Grimholt & Skogestad, 2012).

Although two-degree-of-freedom (DoF) IMCs result in good tracking and disturbance rejection (Kaya, 2004; Li et al., 2021), multi-loop structures with reference models are also used to improve the disturbance rejection of PIDs (Alagoz et al., 2020). The IMC has already been combined with other MBCs, such as the MRC (Ogata, 1997) and its adaptive variant (MRAC) (Galvão & Hadjiloucas, 2019; Marusak & Kuntanapreeda, 2015). The IMC has also been combined with neural networks using rallying models (Rivals & Personnaz, 2000).

High transmission ratios in manipulators make the variable torques caused by the kinematic chain almost negligible for independent joint control (IJC); however, there are cases in which they have to be compensated for, e.g., mobile robots requiring their wheels to rotate fast. This work combines the MRC with the IMC to improve the speed control of a direct current (DC) motor and make it behave as a reference model, especially for IJC when load variation and disturbances are present.

This work proposes a motor speed control scheme that combines the MRC with the IMC and compares three different versions of it, namely Proportional (P), Integral (I), and Proportional-Integral (PI) controllers, with the PID controller. The main research objective is to design the controller and evaluate the best type of control action that can be used to compensate for the deviation with respect to the reference model under setpoint changes. The three different versions of the proposed controller are compared with the PID controller using a simulated DC motor model. The control action with the best performance is then validated with a physical DC motor and compared with the conventional PID. Although nested loops and cascade control schemes are consolidated approaches for motor

https://doi.org/10.24846/v32i2y202306

control using electrical drives, the proposed method allows using more basic H-bridges and control devices.

This paper is organized as follows: Section 2 introduces the IMC, the MRC, and the DC motor models. The proposed scheme is presented in Section 3. Section 4 compares the experimental results obtained with the proposed structure and the PID. Conclusions are presented in Section 5.

2. Theoretical Background

This section introduces the IMC, the MRC, and the DC motor model.

2.1 IMC-based PID (IMC-PID)

The basic IMC structure can be rearranged into a standard feedback structure (Rivera, Morari & Skogestad, 1986) with a controller $Q_{IMC}(s)$, a disturbance $D(s)$, the process $G_p(s)$, a model of the process $\tilde{G}_p(s)$, and a second controller defined by:

$$Q(s)=\frac{Q_{IMC}(s)}{1-\tilde{G}_p(s)Q_{IMC}(s)} \tag{1}$$

An IMC-PID can control a DC motor modeled by:

$$\tilde{G}_p(s)=\frac{k_p}{(\tau_1 s+1)(\tau_2 s+1)} \tag{2}$$

Since the IMC-PID and the direct synthesis method (Kumar, Singla & Chopra, 2015) result in the same controller, it can be said that $\tilde{G}_p(s)=G_p(s)$. This means the real closed-loop response $Y(s)$ will be the same as the desired first-order closed-loop response given by equation (3) when the controller in (4) is used.

$$G_m(s)=\frac{Y(s)}{R(s)}=\frac{1}{\lambda s+1} \tag{3}$$

$$Q(s)=\left(\frac{\tau_1+\tau_2}{k_p\lambda}\right)\frac{\tau_1\tau_2 s^2+(\tau_1+\tau_2)s+1}{(\tau_1+\tau_2)s} \tag{4}$$

The tuning parameters of $Q(s)$ are:

$$k_c=\frac{\tau_1+\tau_2}{k_p\lambda} \tag{5}$$

$$\tau_I=\tau_1+\tau_2 \tag{6}$$

$$\tau_D=\frac{\tau_1\tau_2}{\tau_1+\tau_2} \tag{7}$$

2.2 MRC Strategy

The MRC uses a model to define the desired system response and the error between both outputs to generate a control signal (Ogata, 1997). It is possible to find schemes that do not include adaptation mechanisms (Moctezuma & Sánchez, 2011). However, there are also some that do (Butler, 1990), such as the popular scheme illustrated in Figure 1.

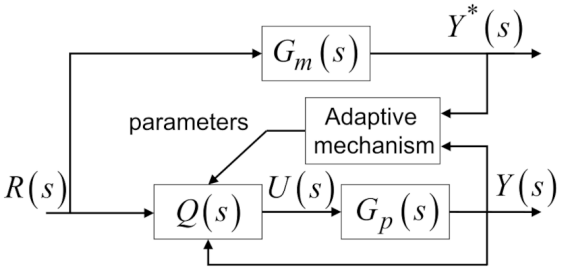

Figure 1. General Model Reference Adaptive Control (MRAC) scheme

2.3 DC Motor Model

The state space model of the DC motor, as seen in equation (8), can be obtained from the diagram displayed in Figure 2. The parameters in Table 1 help to describe how the DC voltage $v(t)$, the angular speed $\omega(t)$, the armature current $i(t)$, the back electromotive force (EMF) $v_b(t)$ from equation (9), and the load torque $T_L(t)$ are related.

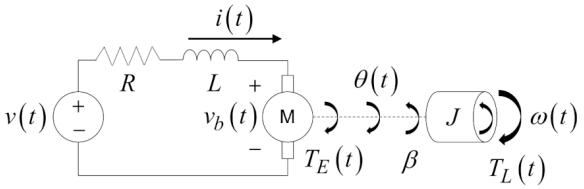

Figure 2. Electromechanical model of the DC motor

Table 1. Parameters used to simulate a DC motor

	Parameter	Value
L	Armature inductance	$5.8\times10^{-4}\,H$
R	Armature resistance	5.3Ω
J	Rotor inertia	$1.4\times10^{-6}\,kg\,m^2$
β	Friction coefficient	$2.0126\times10^{-6}\,N\,m\,s$
k_t	Torque constant	$2.2\times10^{-2}\,N\,m/A$
k_b	Back EMF constant	$2.2\times10^{-2}\,V\,s/rad$

There are procedures to obtain the motor parameters, as the one reported in (Monasterio-Huelin & Gutiérrez, 2020). Some parameters can be obtained experimentally, but others need to be calculated.

$$\begin{bmatrix}\dot{\theta}(t)\\ \dot{\omega}(t)\\ \dot{i}(t)\end{bmatrix}=\begin{bmatrix}0 & 1 & 0\\ 0 & -\beta/J & k_t/J\\ 0 & -k_b/L & -R/L\end{bmatrix}\begin{bmatrix}\theta(t)\\ \omega(t)\\ i(t)\end{bmatrix}+\begin{bmatrix}0 & 0\\ 0 & -1/J\\ 1/L & 0\end{bmatrix}\begin{bmatrix}v(t)\\ T_L(t)\end{bmatrix} \tag{8}$$

$$v_b(t)=k_b\omega(t) \tag{9}$$

The resulting transfer functions including ω are:

$$\frac{\omega(s)}{V(s)}=\frac{k_t}{JLs^2+JRs+L\beta s+\beta R+k_tk_b} \tag{10}$$

$$\frac{\omega(s)}{T_L(s)}=\frac{-(Ls+R)}{JLs^2+JRs+L\beta s+\beta R+k_tk_b} \tag{11}$$

2.4 Discrete-Time Equations

The motor model and the IMC-PID can be discretized using the following equation for the backward Euler method, where T_s represents the sampling time:

$$s\approx\frac{1-z^{-1}}{T_s} \tag{12}$$

Using the superposition principle, equations (10) and (11) lead to:

$$\omega_n=\frac{\left(k_tv_n-RT_{L_n}\right)T_s-L\left(T_{L_n}-T_{L_{n-1}}\right)}{\frac{JL}{T_s}+JR+\beta L+\left(\beta R+k_tk_b\right)T_s}+\frac{\left(JR+\beta L+\frac{2JL}{T_s}\right)\omega_{n-1}-\frac{JL}{T_s}\omega_{n-2}}{\frac{JL}{T_s}+JR+\beta L+\left(\beta R+k_tk_b\right)T_s} \tag{13}$$

The resulting difference equation for the IMC-PID controller is:

$$u_n=\tau_1\tau_2\left(\frac{e_n-2e_{n-1}+e_{n-2}}{k_p\lambda T_s}\right)+\frac{(\tau_1+\tau_2)(e_n-e_{n-1})+e_nT_s}{k_p\lambda}+u_{n-1} \tag{14}$$

3. Proposed MRC-IMC Control Scheme

As mentioned in Section 1, a robot generates a variable load torque when it moves, and there are situations in which this has to be considered for IJC. The IMC results in robust controllers when the model constitutes a good approximation, which does not happen when the DC motor is affected by a variable torque.

3.1 MRC-IMC Controller Design

To improve the system response, this work proposes combining the IMC-PI and the MRC; this is done by including a reference model $G_m(s)$ to define the expected closed-loop behavior $Y^*(s)$ and an additional controller $G_{MRC}(s)$ to deal with the difference between $Y^*(s)$ and $Y(s)$. This research is particularly interested in finding the best type of contribution (P, I, or PI) for the MRC controller that compensates for a variable torque T_L. The proposed scheme is shown in Figure 3.

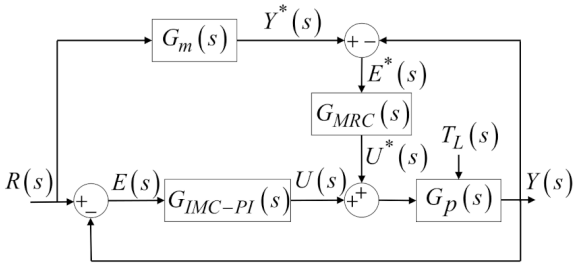

Figure 3. Proposed MRC-IMC scheme

To impose a first-order behavior on the DC motor control system, $G_m(s)$ is defined as in equation (3); the same desired closed-loop time constant, λ, is used in $G_{IMC-PI}(s)$ and $G_m(s)$. The difference equations (13) and (15) are for $G_p(s)$ and $G_m(s)$, respectively. Lastly, the difference equation for $G_{IMC-PI}(s)$ is obtained by substituting $\tau_1=\tau_p$ and $\tau_2=0$ into equation (14), which results in equation (16).

$$y_n^*=\frac{T_sr_n+\lambda y_{n-1}^*}{\lambda+T_s} \tag{15}$$

$$u_n=\frac{(\tau_p+T_s)e_n-\tau_pe_{n-1}}{k_p\lambda}+u_{n-1} \tag{16}$$

Although the setpoint is defined in the diagrams as $R(s)$ and the output as $Y(s)$, this work studies the speed control of a DC motor, which means that they refer to angular velocities; because of this, they could be defined as $\omega^*(s)$ and $\omega(s)$, respectively.

3.2 Simulation and Experimental Setup

Five tests were carried out using LabVIEW to control the plant; three of them also simulated a DC motor using equation (13) and the parameters from Table 1.

The tests with a simulated DC motor compared three $G_{MRC}(s)$ controllers, a PI, a P, and an I. The PI contributions from the MRC were defined in terms of K_p and K_i, the proportional and integral gains, respectively (with capital letters to distinguish them from those of the IMC); the controller transfer function and discretization are:

$$G_{MRC-PI}(s) = \frac{K_p s + K_i}{s} \tag{17}$$

$$u_n^* = K_p\left(e_n^* - e_{n-1}^*\right) + K_i T_s e_n^* + u_{n-1}^* \tag{18}$$

The P and I controllers from equations (19) and (20) are obtained by substituting $K_i = 0$ and $K_p = 0$ into equation (18), respectively.

$$u_n^* = K_p e_n^* \tag{19}$$

$$u_n^* = K_i T_s e_n^* + u_{n-1}^* \tag{20}$$

The alternative with the PI was used to control a real DC motor because, as it will be shown in subsection 4.1, the results obtained with it were better than the ones obtained with the P and I controllers. A PID controller was also used in all the tests and was tuned as an IMC-PID for the simulated DC motor, and by using particular tuning parameters for the real one. For a better comparison, three performance indexes were computed, these are: the control signal total variation (TV_u), the integral of time multiplied by the squared error ($ITSE$), and the integral of the absolute magnitude of the error (IAE). Their discrete equivalents, adapted from (de Moura Oliveira, Hedengren & Solteiro Pires, 2020), where N is the number of samples, are:

$$TV_u = \sum_{k=1}^{N} \left|u_k - u_{k-1}\right| \tag{21}$$

$$ITSE = \sum_{k=0}^{N} k\, e^2(k) T_s^2 \tag{22}$$

$$IAE = \sum_{k=0}^{N} \left|e(k)\right| T_s \tag{23}$$

The TV_u index compares the control signals and shows which scheme applies less voltage variation to the motor; in this work, the first two values were not used for the results not to be affected by the initial peaks, even if they are presented in the plots. The $ITSE$ and IAE indexes compare the errors to understand which scheme is best at setpoint tracking.

3.2.1 Simulated DC Motor Setup

Test A was done without load torque ($T_L = 0Nm$); this was added in Test B as a triangular signal with an amplitude of $0.001Nm$, a frequency of $10Hz$, and without offset. The T_L used in Test C mixed 50% of the triangular signal and 50% of random noise with a maximum value of $0.001Nm$.

Each test lasted $0.3s$ with $T_s = 0.0001s$; for them, the setpoint was set to $100rad/s$ before running the program. The following parameters were used for the MRC-IMC and the PID (which was tuned using the IMC principle):

- PID and MRC-IMC structures: $\lambda = 0.02s$;
- PID: $k_p = 44.4744$, $\tau_1\tau_2 = 1.64151\times10^{-6}$ and $\tau_1 + \tau_2 = 0.0150024$;
- MRC-IMC structures: $k_p = 44.4744$, $\tau_p = 0.015$, $K_p = 0.2$ and $K_i = 44.4744$.

The MRC-IMC gains were defined when the triangular T_L was applied; the IMC-PI parameters were used as reference values. In the case of $K_i = k_p$, the scheme using the I controller showed that higher and lower values lead to an increase in the TV_u; however, there exists a range of K_i that gives similar results. The scheme with the P controller was used to define $K_p = 10\lambda$ and showed that smaller values increase the amplitude of the oscillations of ω, while higher values increase the TV_u. These gains were also selected for the PI because they result in smaller $ITSE$ and IAE values compared with the other controller variants. It was seen that lower values of K_i increase the $ITSE$ and IAE, and higher values only reduce them slightly. With respect to K_p, smaller values make the closed-loop response more similar to the one of the I controller, and higher values drastically increase the TV_u.

3.2.2 Real DC Motor Setup

A small DC motor with an encoder was used to try to make it behave during acceleration in the same way it behaves while decelerating, which does not happen due to the different loads present

in both situations. While Test D did not involve an additional load, an extreme load variation was used in Test E.

Besides the DC motor, this test used an L298N driver, an NI myRIO (acting as the rest of the control system), and a $12V$ power supply; the connection diagram of the system can be seen in Figure 4. The control signal sent to the DC motor is the minimum of the computed one and the voltage provided by the power supply.

Before controlling the DC motor, an approximated first-order model was identified using an open-loop scheme and the $12V$ power supply. The gain and time constant of the model are $k_m \approx 1$ and $\tau_m \approx 0.045s$, respectively.

The setpoint changes used in Test D were from $0 rad/s$ to $10 rad/s$ and from $10 rad/s$ to $5 rad/s$; for Test E they were from $0 rad/s$ to $5 rad/s$ and from $5 rad/s$ to $3 rad/s$. For each, 500 samples were obtained with $T_s = 0.01s$.

The following parameters were used because they allowed obtaining similar responses with both schemes:

- PID and MRC-IMC structures: $\lambda = 0.1s$;
- PID: $k_p = k_m = 1$ and $\tau_1 = \tau_2 = \tau_m = 0.045s$;
- MRC-IMC structure: $k_p = k_m = 1$, $\tau_p = \tau_m = 0.045s$, $K_p = 2$ and $K_i = 2$.

As a result, the PID tuning parameters were defined as: $\tau_I = 2\tau_m$, $\tau_D = 0.5\tau_m$, and $k_c = \tau_m / (k_m \lambda)$.

4. Results and Discussion

This section presents the results obtained with each test.

As mentioned before, to tune the MRC-IMC, it is suggested to start with $K_p = 10\lambda$ and $K_i = k_m$; these gains can be manually fine-tuned afterward. The value of K_i can be increased until the error is within the desired threshold, but it is recommended to do this gradually, because large values can lead to instability. Overshoots can be dealt with by increasing K_p in the $G_{MRC}(s)$ controller; however, the simulations showed that this significantly increases the TV_u.

4.1 Results with a Simulated DC Motor

The first test was done to validate if the proposed control strategy has at least a similar response to a PID, which typically has good performance for constant load torque. In Test A, the behavior obtained with the three MRC-IMC variations and the PID control did not present visible differences in performance for setpoint tracking. The control signals sent to the simulated motor during the first $0.1s$ are shown in Figure 5; visible differences exist during the rise time of the angular velocities, especially for the MRC-IMC with the I controller, which presents oscillations at the beginning, and for the PID, which presents an initial peak.

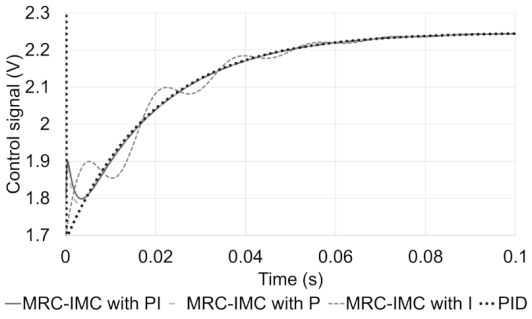

Figure 5. Control signals generated in Test A

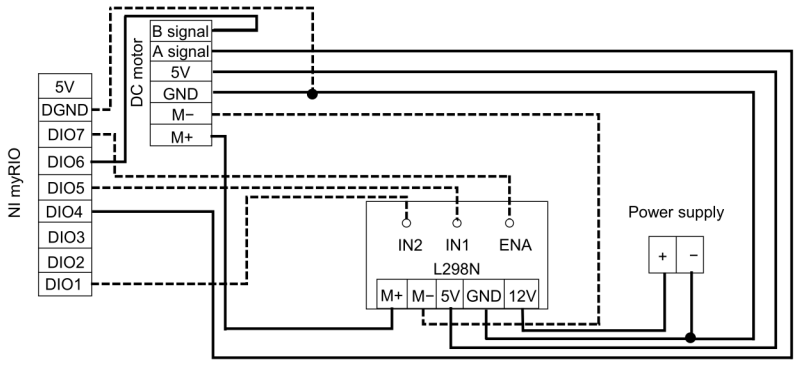

Figure 4. Connection diagram of the system used for the experimental setup

The performance indexes in Table 2 show that the MRC-IMC with the I controller results in the lowest $ITSE$, while the PID has the lowest TV_u value. With this test, it is possible to conclude that MRC-IMC and PID controllers have comparable performance when no T_L is applied, which validates the applicability of the MRC-IMC schemes.

Table 2. Performance indexes computed for Test A

Scheme	TV_u	$ITSE$	IAE
MRC-IMC with PI	0.5918	0.994148	2
MRC-IMC with P	0.59129	0.994478	2.00036
MRC-IMC with I	0.68595	0.993832	2
PID	0.55709	0.994994	2

The second test was intended to evaluate the performance of the proposed controllers under load variations and compare them with a PID. Figure 6 shows the closed-loop responses obtained in Test B; these show that the MRC-IMC strategies are better at setpoint tracking and regulatory control. However, the MRC-IMC with the PI and I controllers behave better than the rest, as proved by the zoom-in presented in Figure 7, which also shows that the best behavior is obtained with the PI.

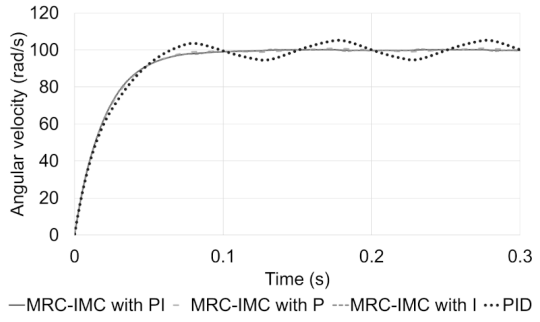

Figure 6. Outputs of the control schemes during Test B

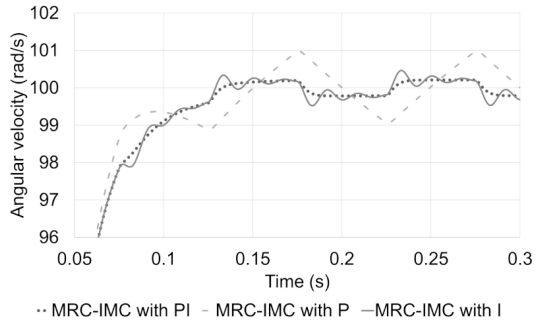

Figure 7. Zoom-in of the outputs of the MRC-IMC schemes during Test B

It can be seen that the results in Table 3 support the previous discussion about Test B because the $ITSE$ and IAE values for the MRC-IMC with the PI and I controllers are the lowest. The performance indexes also show that the PID requires the lowest voltage variation and the MRC-IMC with the I controller the highest. The control signals can be observed in Figure 8 (as it can be noticed, the PID controller generates an initial voltage peak). With this test, better performance of the proposed MRC-IMC control schemes can be observed compared to the PID in the case of load variations.

Table 3. Performance indexes computed for Test B

Scheme	TV_u	$ITSE$	IAE
MRC-IMC with PI	3.169	0.996012	2.03131
MRC-IMC with P	2.82444	1.03017	2.09402
MRC-IMC with I	3.25133	0.995496	2.03794
PID	1.82668	1.62169	2.69083

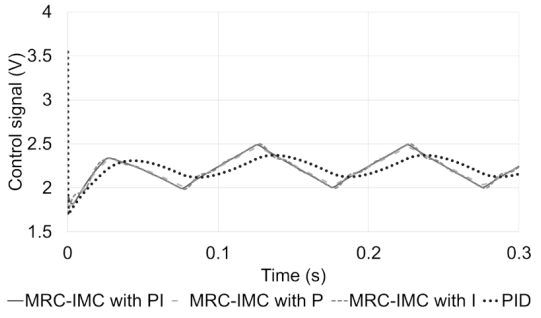

Figure 8. Control signals generated during Test B

The third test was meant to compare the proposed schemes under a stochastic load variation scenario. The system responses from Test C presented similar behavior to those in Figure 6, which means that the MRC-IMC strategies are better at setpoint tracking and regulatory control even when T_L presents random variations. The zoom-in presented in Figure 9 proves that the behavior obtained using the PI is slightly better than the one with the I controller and that both are better than the one with the P controller; as it can be seen in Table 4, the MRC-IMC schemes with the PI and I controllers result in the lowest $ITSE$ and IAE values. The performance indexes also prove that the PID requires the lowest voltage variation and that the MRC-IMC with the PI and the P controllers need more than the alternative with the I controller. The control signals generated during Test C were similar to the ones of Test B, illustrated in Figure

8. From this test, it can be observed that the MRC-IMC schemes perform better than the PID. The MRC-IMC with a PI contribution is the scheme with the best overall performance because it gives a maximum error of only $\pm 0.2\%$.

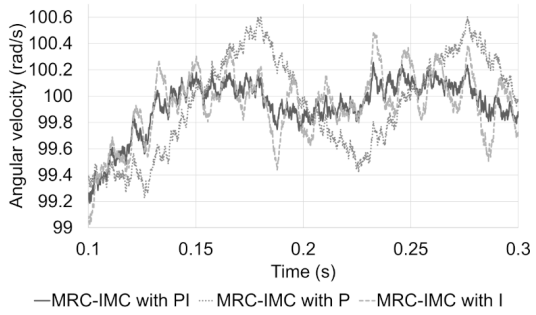

Figure 9. Zoom-in of the outputs of the MRC-IMC control schemes during Test C

Table 4. Performance indexes computed for Test C

Scheme	TV_u	*ITSE*	*IAE*
MRC-IMC with PI	12.11795	0.994809	2.0154
MRC-IMC with P	11.87975	1.00937	2.04877
MRC-IMC with I	2.56368	0.994916	2.0253
PID	2.42967	1.18149	2.3126

4.2 Results with a Real DC Motor

From simulation results, the MRC-IMC with a PI contribution can be regarded as a good control scheme when a variable load is present. Experimental tests were necessary to validate its performance with a real DC motor. For a fair comparison, the parameters of both schemes, the PID and the MRC-IMC, were manually adjusted to improve their performance and find comparable responses (see subsection 3.2.2).

As previously mentioned, the control signals were limited to $12V$ when higher values were computed, which happened with the PID at the beginning of each test. However, this will not be shown in the plots because the data were filtered for better visualization; these high voltages did not affect the TV_u values because, as said before, the first two values were not used to compute it.

The angular velocities from Test D are presented in Figure 10, while Figure 11 shows the generated control signals, which present peaks when the setpoint is changed; the data in said plots were filtered using equation (24). Although both control schemes are good at setpoint tracking, Table 5 shows that the PID has lower *ITSE* and *IAE* during deceleration and that the MRC-IMC always requires less voltage variations.

$$x_{\text{filtered}} = 0.5\, x_{i-1} + 0.5\, x_i \tag{24}$$

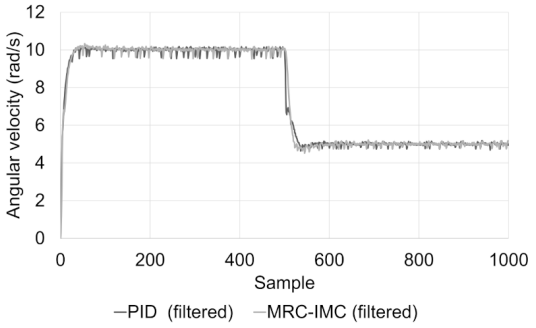

Figure 10. Filtered angular velocities obtained during Test D

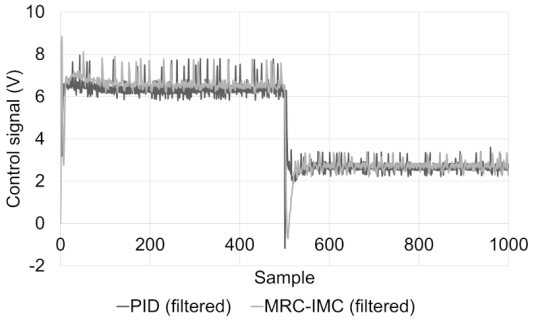

Figure 11. Filtered control signals generated during Test D

Table 5. Performance indexes for Test D computed using unfiltered data

Index	Acceleration		Deceleration	
	MRC-IMC with PI	PID	MRC-IMC with PI	PID
TV_u	297.11064	589.22415	205.6362	364.089398
ITSE	0.756585	0.820309	0.353242	0.311624
IAE	1.51967	1.43043	1.09523	0.942453

The angular velocities obtained during Test E, by using an extreme load variation, are shown in Figure 12, while Figure 13 shows the control signals, with voltage peaks existing at each setpoint change; as in the previous test, these present filtered data. Both control schemes are similar at setpoint tracking and regulatory control; however, the *ITSE* and *IAE* values in Table 6 prove that the MRC-IMC has a better response and requires less voltage variations when an additional load is present.

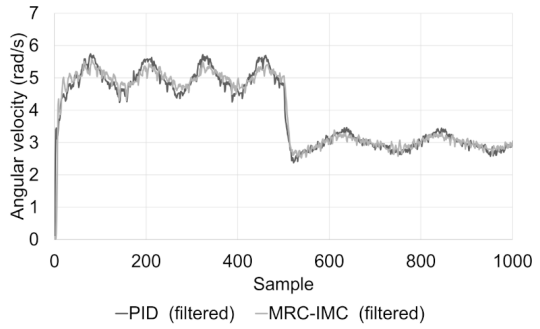

Figure 12. Filtered angular velocities obtained during Test E

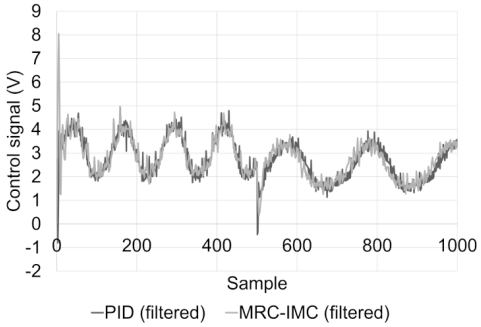

Figure 13. Filtered control signals generated during Test E

4.3 Discussion of Main Results

The proposed MRC-IMC scheme intends to improve the speed control of DC motors and compensate for load variations, which are present in some mechatronic and robotic applications. A conventional IMC-PID was chosen for the comparisons using the simulated DC motor because this type of controller is widely used to control the speed of motors. Test A was designed to validate the performance of the proposed scheme under constant torque. Test B and Test C were defined to compare the performance of the control schemes under variable load scenarios and proved that the proposed MRC-IMC strategies performed better than the PID; Test C also showed that, under stochastic load variations, the MRC-IMC with a PI contribution is the best alternative.

Experimental tests were carried out to evaluate and validate the performance of the proposed scheme. For these tests, the MRC-IMC and PID were tuned up for a comparable performance under an extreme load variation scenario; as a result, suitable tuning parameters were chosen for the PID, which can be considered a finding of this research work. However, even with those novel parameters, the proposed MRC-IMC with a PI contribution results in a slightly better performance. Test D also showed that both schemes allow the behavior of the motor to be similar during acceleration and deceleration.

5. Conclusion

The IMC principle allows obtaining a relatively robust controller that can be implemented as an IMC-PID controller; however, particular applications require multi-loop strategies for better perturbation rejection. This work proposes combining an IMC-PI and an additional PI controller that considers the deviation from a reference model.

Different MRC controllers (P, I, and PI) were designed to control a simulated DC motor. The closed-loop responses validated that the MRC-IMC schemes lead to better setpoint tracking and regulatory control than an IMC-PID when the

Table 6. Performance indexes for Test E computed using unfiltered data

Index	Acceleration		Deceleration	
	MRC-IMC with PI	PID	MRC-IMC with PI	PID
TV_u	203.610124	335.33657	152.129658	278.50467
ITSE	0.860165	1.97186	0.430551	0.654688
IAE	1.4439	1.92544	0.94091	1.04767

non-negligible load torque is variable. Tuning criteria were defined for the MRC controllers.

An experimental setup was implemented with a DC motor to evaluate the performance of the proposed strategy and compare it with a conventional PID. Particular tuning parameters suitable for motor control under variable torque were found for the PID; these are $\tau_I = 2\tau_m$, $\tau_D = 0.5\tau_m$, and $k_c = 2\tau_m / (k_m \lambda)$. Experimental results showed good performance with both schemes, PID (tuned with the previously described parameters) and MRC-IMC with a PI; the latter showed smaller errors in most of the performed tests and always required less voltage variations.

The proposed MRC-IMC scheme has the advantages of imposing a first-order response to the actuator and improving its closed-loop response by better compensating for load disturbances. It was proved that the MRC-IMC scheme is helpful for DC motor speed control applications involving non-negligible variable load torques, which are present in some mechatronic and robotic systems with low gear ratios at their prismatic and rotational joints. The intended future work will use the proposed MRC-IMC scheme to implement IJC for the inverse kinematic control of a 6-DoF articulated robot.

Acknowledgements

The research presented in this paper has been funded by the National Council of Science and Technology (Consejo Nacional de Ciencia y Tecnología – CONACYT), Mexico.

REFERENCES

Alagoz, B. B., Tepljakov, A., Petlenkov, E. & Yeroglu, C. (2020) Multi-loop model reference proportional integral derivative controls: design and performance evaluations. *Algorithms.* 13(2), 38. doi: 10.3390/a13020038.

Arenas-Rosales, F., Martell-Chávez, F. & Sánchez-Chávez, I. Y. (2022) Discrete time DC motor model for load torque estimation for PID-IMC speed control. *Mechatronic Systems and Control.* 50(2), 102-108. doi: 10.2316/J.2022.201-0265.

Butler, H. (1990) *Model reference adaptive control: Bridging the gap between theory and practice*. PhD thesis. Delft University of Technology (TU Delft).

de Moura Oliveira, P. B., Hedengren, J. D. & Solteiro Pires, E. J. (2020) Swarm-based design of proportional integral and derivative controllers using a compromise cost function: An Arduino temperature laboratory case study. *Algorithms.* 13(12), 315. doi: 10.3390/a13120315.

Dermitas, M. (2011) Off-line tuning of a PI speed controller for a permanent magnet brushless DC motor using DSP. *Energy Conversion and Management.* 52(1), 264-273. doi: 10.1016/j.enconman.2010.06.067.

Galvão, R. K. & Hadjiloucas, S. (2019) Measurement and control of emergent phenomena emulated by resistive-capacitive networks, using fractional-order internal model control and external adaptive control. *Review of Scientific Instruments.* 90(10), 103003. doi: 10.1063/1.5097743.

Grimholt, C. & Skogestad, S. (2012) Optimal PI-control and verification of the SIMC tuning rule. In: Vilanova, R. & Visioli, A. (eds.) *Proceedings of the 2nd IFAC Conference on Advances in PID Control, PID'12 2012, 28 – 30 March 2012, Brescia, Italy.* New York, USA, Elsevier. pp. 11-22.

Kaya, I. (2004) Two-degree-of-freedom IMC structure and controller design for integrating processes based on gain and phase-margin specifications. *IEE Proceedings-Control Theory and Applications.* 151(4), 481-487. doi: 10.1049/ip-cta:20040658.

Kumar, R., Singla, S. K. & Chopra, V. (2015) Comparison among some well known control schemes with different tuning methods. *Journal of Applied Research and Technology.* 13(3), 409-415. doi: 10.1016/j.jart.2015.07.007.

Li, R., Zhu, Q., Narayan, P., Yue, A., Yao, Y. & Deng, M. (2021) U-model-based two-degree-of-freedom internal model control of nonlinear dynamic systems. *Entropy.* 23(2), 169. doi: 10.3390/e23020169.

Marusak, P. M. & Kuntanapreeda, S. (2015) Output constrained IMC controllers in control systems of electromechanical actuators. *Control Theory and Technology.* 13(3), 245-255. doi: 10.1007/s11768-015-4047-0.

Moctezuma, R. A. G. & Sánchez, A. C. (2011) Algebraic identification of a DC servomechanism using a Least Squares algorithm. In: *Proceedings of the 2011 American Control Conference, ACC 2011, 29 June – 01 July 2011, San Francisco, CA, USA*. Piscataway, Institute of Electrical and Electronics Engineers (IEEE). pp. 102-106.

Monasterio-Huelin, F. & Gutiérrez, A. (2020) *Modeling of a DC motor. [Modelado de un motorDC]*. Madrid, Robolabo, The Technical University of Madrid (Universidad Politécnica de Madrid – UPM). http://www.robolabo.etsit.upm.es/asignaturas/seco/apuntes/2019-2020/modelado.pdf [Accessed 29th April 2022].

Najafi, A. & Spencer Jr., B. F. (2019) Adaptive model reference control method for real-time hybrid simulation. *Mechanical Systems and Signal Processing.* 132, 183-193. doi: 10.1016/j.ymssp.2019.06.023.

Normey-Rico, J. E. & Camacho, E. F. (2007) *Control of Dead-time Processes.* London, Springer.

Ogata, K. (1997) *Modern Control Engineering.* New Jersey, Prentice Hall.

Ren, Y., Wang, R., Rind, S. J., Zeng, P. & Jiang, L. (2022) Speed sensorless nonlinear adaptive control of induction motor using combined speed and perturbation observer. *Control Engineering Practice.* 123, 105166. doi: 10.1016/j.conengprac.2022.105166.

Rivals, I. & Personnaz, L. (2000) Nonlinear internal model control using neural networks: Application to processes with delay and design issues. *IEEE Transactions on Neural Networks.* 11(1), 80-90. doi: 10.1109/72.822512.

Rivera, D. E., Morari, M. & Skogestad, S. (1986) Internal model control: PID controller design. *Industrial & Engineering Chemistry Process Design and Development.* 25(1), 252-265. doi: 10.1021/i200032a041.

Yao, J., Jiao, Z. & Ma, D. (2014) Adaptive robust control of DC motors with extended state observer. *IEEE Transactions on Industrial Electronics.* 61(7), 3630-3637. doi: 10.1109/TIE.2013.2281165.

Zhen, S., Hao, J., Liu, X., Wu, Q., Zhao, H. & Chen, Y. H. (2022) A practical robust bounded control for permanent magnet linear motor with inequality constraints. *Control Engineering Practice.* 122, 105068. doi: 10.1016/j.conengprac.2022.105068.